Swansea University
Prifysgol Abertawe

Cronfa
Setting Research Free

Cronfa - Swansea University Open Access Repository

This is an author produced version of a paper published in :
Computers & Structures

Cronfa URL for this paper:
http://cronfa.swan.ac.uk/Record/cronfa31964

Paper:
Wang, C., Khodaparast, H., Friswell, M. & Shaw, A. (2017). An equivalent model of corrugated panels with axial and bending coupling. *Computers & Structures, 183*, 61-72.
http://dx.doi.org/10.1016/j.compstruc.2017.01.008

This article is brought to you by Swansea University. Any person downloading material is agreeing to abide by the terms of the repository licence. Authors are personally responsible for adhering to publisher restrictions or conditions. When uploading content they are required to comply with their publisher agreement and the SHERPA RoMEO database to judge whether or not it is copyright safe to add this version of the paper to this repository.
http://www.swansea.ac.uk/iss/researchsupport/cronfa-support/

An equivalent model of corrugated panels with axial and bending coupling

Chen Wang, Hamed Haddad Khodaparast, Michael Ian Friswell, Alexander David Shaw
College of Engineering, Swansea University, United Kingdom

Abstract

In this paper, modification of an existing equivalent model of the corrugated panel is investigated. The axial and bending coupling of the corrugated panel supplements the previous equivalent properties when the corrugated panel has a fixed boundary condition. The analytical expressions of the coupling vertical deflections are obtained and verified by the finite element method. A method to eliminate the vertical deflection is proposed, and the importance of the coupling effect is demonstrated by the application of the modified model in a compliant structure.

Key words: Corrugated panel, Equivalent model, Coupling, Analytical solution

1. Introduction

Corrugated panel is made of plate with periodic profiles. Corrugated panels can be used as cores in sandwich structures. Although the finite element method can be used to evaluate the stiffness of the corrugated structures, the detailed modelling of the profiles will lead to a high computation cost, which motivates the study of equivalent models [1-3].

In recent years the study of morphing aircraft becomes another motivation of the research into corrugated structures [4-6]. The low axial stiffness of the corrugated structure allows for a large deformation with limited actuation force while the high anisotropy of the corrugated structure still provides a large out-of-plane stiffness to carry aerodynamic loads.

The study of equivalent models of corrugated panels plays a significant role in research and applications. Yokozeki et al. [4] developed the analytical solution of the equivalent axial and transverse tensile and flexural modulii with the round corrugation. The analytical solution provided a reasonable accuracy compared to the experimental results. Samanta and Mukhopadhyay [7] derived analytical solutions of the axial and transverse equivalent modulii of the trapezoidal corrugated panel. The experimental investigation of Thill et al. [8] showed a three-stage stress-strain relationship of the trapezoidal corrugated panel, in which the first linear stage had a relatively good agreement with the analytical solution modified from [7]. Xia et al. [9] developed a more complete approach of the corrugated panel, which gives the equivalent model of round and trapezoidal corrugations. The method provides the closed forms of the six effective components in the stiffness matrix of the equivalent orthotropic plate. Comparisons to other analytical results and the finite element method have shown the accuracy of the equivalent model. In this method, the equivalent orthotropic plate is a classical Kirchhoff plate, which does not consider the transverse shear. A recent publication from Mohammadi et al. [10] derived the transverse shear modulus, which few researchers have studied. The equivalent models of corrugated cores with elastomeric coatings were also derived by Dayyani et al. [11].

Although the equivalent properties of the corrugated panel have been studied extensively, this paper investigates another aspect, namely the axial and bending coupling when the corrugated panel has a fixed boundary condition, to which little attention has been paid in the literature. The corrugated panel will have a vertical deflection caused by the pure extension load when it has a fixed boundary condition.

If the corrugated panel has a pinned boundary condition, no vertical deflection will occur. This deflection-extension coupling effect could be negligible in some cases. But it can also have significant influence on the entire structure, especially for the morphing applications where the corrugated structures are often required to have a relatively large deformation. For example, if the corrugated structure is used as the morphing skin, the tendency of the out-of-plane deflection could change the wing shape or increase the actuation energy. The current investigation can also provide guidelines for installing the corrugated panels in real-world applications. In the previous references, the symmetry of the structure is usually applied and only half [7] or quarter [4, 10] of the corrugation unit is analysed. The fixed boundary condition is applied to calculate the strain energy and internal moment. For the homogeneous method [9] the boundary condition will not affect the equivalent properties of the entire structure since the boundary conditions are constrained when calculating the strain energy.

In this paper, with the fixed boundary condition, vertical deflections under pure extension load will be analysed together with axial deflections. The axial deflections are applied to calculate the equivalent axial modulii, which are compared to those from the existing models. The coupling effect can be represented as an effect of the boundary condition if the entire corrugated panel is separated into two segments. As a supplement to the previous equivalent model, a modification to the equivalent model proposed in the reference [9] is made by introducing a coupling component. After representing this deflection, the influence of considering this coupling effect is shown on its potential application to a compliant structure. The method to eliminate this coupling is also proposed by using an offset boundary condition.

2. Deflections caused by extension loads

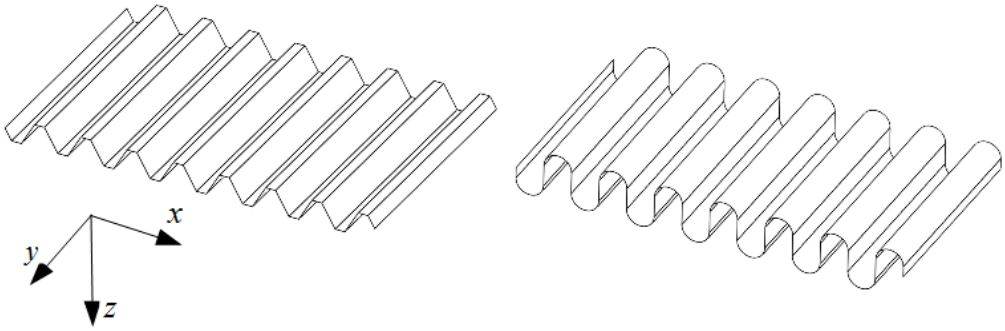

Figure 1. (a): trapezoidal corrugation panel, (b): round corrugation panel

Figure 1 shows the shape of the trapezoidal and round corrugation panels, which are the subject of this study. As a periodic structure in the *xz* plane, the entire shape and size of a corrugated structure is determined by the shape of a basic single unit and the number of units.

Figure 2 shows the unit geometry and the internal bending moment for the corrugated shapes. The corrugation unit is fixed at one end and under extension load T at the other end. As shown in the figure, the trapezoidal unit consists of the straight beams AB, BC, CD, DE, EF and FG, and the round unit is made of straight beams AB, CD, EF and curved beams BC, DE.

The deflection of each separate beam is calculated using classical mechanics and Castigliano's second theorem. The deflection of the unit corrugation is then calculated by accumulating the local deflections of the beams and considering the rigid translation caused by the rotation angles of the beam cross sections. Figure 3 shows the schematic of the deflection components. For a beam with the inclined angle θ, the deflection of the beam p, which is perpendicular to the beam, can be decomposed to the

axial deflections u and the vertical direction w. According to the inclined angle and direction definition, we have $u = -p\sin\theta$, and $w = p\cos\theta$. Also, the rotation angle of the beam cross section will lead to a rigid translation. The rotation angle α of an axial beam will cause a vertical deflection w and an axial deflection u can be obtained if the rotation angle occurs in a vertical beam. The axial and vertical deflections of the trapezoidal and round corrugation unit are calculated using the method.

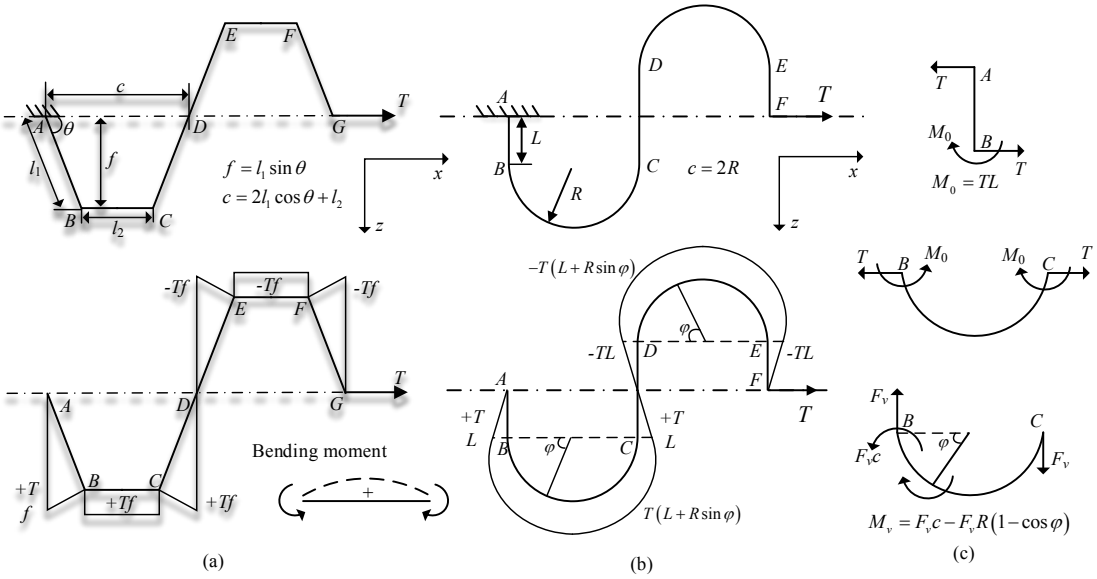

Figure 2. Geometry and bending moment in the corrugation unit: (a): trapezoidal, (b): round, (c): separate beams in the round unit

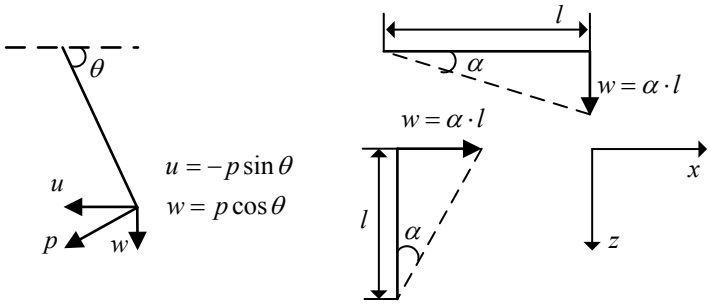

Figure 3. Schematic of the deflection components

As shown in Figure 2 (a), l_1, l_2 and θ are the length of beams AB and BC, and the inclined angle respectively in the trapezoidal corrugation. The shape of the trapezoid can also be represented by the length c and the height f. These beams are rigidly connected to the previous part and thus the global vertical deflection of a point depends on the deformation on the previous beams. For example the deflection of point C includes three parts: the global vertical deflection of point B, the local vertical deflection of beam BC and the rigid translation of point B caused by the rotation angle of the beam cross section at point B. The rotation angle of the beam cross section will also be accumulated by the local rotation angle. Then, the global vertical deflection of point C, w_C, can be calculated as

$$w_C = w_B + w_{BC} + \alpha_B \cdot l_2 \tag{1}$$

where p, u and w are the deflection value perpendicular to the beam, in the axial or vertical direction respectively. α is the rotation angle of the beam cross section. The subscript 'AB' or 'BC'

means the local deflection or beam cross section rotation angle of that beam, the subscript of a single point '*B*' or '*C*' means the global value at that point.

Thus, w_{BC} is the local vertical deflection of beam *BC*, and w_B and α_B are the global deflection and rotation angle of the cross section of point *B*. Also for local deformation of beams *AB* and *BC*, we have

$$p_{AB} = \frac{Tl_1^3 \sin\theta}{6EI}, \alpha_{AB} = \frac{Tl_1^2 \sin\theta}{2EI} \tag{2}$$

$$\begin{aligned} w_B &= p_{AB}\cos\theta = \frac{Tl_1^3 \sin\theta\cos\theta}{6EI} \\ u_B &= -p_{AB}\sin\theta = -\frac{Tl_1^3 (\sin\theta)^2}{6EI} \end{aligned} \tag{3}$$

$$p_{BC} = \frac{Tl_1 l_2 \sin\theta}{2EI}, \alpha_{BC} = \frac{Tl_1^2 \sin\theta}{2EI} \tag{4}$$

$$\begin{aligned} w_{BC} &= p_{BC}\cos 0 = \frac{Tl_1 l_2 \sin\theta}{2EI} \\ u_{BC} &= p_{BC}\sin 0 = 0 \end{aligned} \tag{5}$$

$$\begin{aligned} w_B &= w_{AB}, u_B = u_{AB} \\ \alpha_B &= \alpha_{AB}, \alpha_C = \alpha_B + \alpha_{BC} \end{aligned} \tag{6}$$

where *E* is the Young's modulus, *I* is the second moment of area and *T* is extension force in the *x* direction. Repeating the above steps for the other beams, the deflections and rotation angle at point *G* can be calculated, which are equal to the deflections and rotation angle of the unit as

$$\begin{aligned} u_{unit} &= u_G = \frac{2}{3}\frac{Tl_1^2 (\sin\theta)^2 (2l_1 + 3l_2)}{EI} \\ w_{unit} &= w_G = \frac{Tl_1 \sin\theta (l_1 + l_2)(l_2 + 2l_1\cos\theta)}{EI} \\ \alpha_{unit} &= \alpha_G = 0 \end{aligned} \tag{7}$$

For the round corrugation, the same approach can be applied to obtain the vertical deflection and rotation angle of a single unit. The geometry and internal bending moment of the round corrugation unit is shown in Figure 2(b). The curved beams are assumed to be thin enough compared to the radius *R*, that the beam theory for a straight beam may be applied. The local vertical deflection of the curved beam *BC* are obtained by the Castigliano's second theorem as

$$\begin{aligned} w_{BC} &= \int_0^{\pi} \frac{M}{EI}\frac{\partial M}{\partial F_v} \cdot Rd\varphi \\ M &= TR\sin\varphi + M_0 + F_v\left[c - R(1-\cos\varphi)\right] \end{aligned} \tag{8}$$

where *M* is the bending moment in the curved beam *BC*, and φ is the current angle with respect to the *x* axis. M_0=*TL*, and F_v is virtual vertical force applied at point *C* to obtain the vertical deflection.

The deflections and rotation angle of a round corrugation unit can be obtained using the same approach to the trapezoidal corrugation as

$$
\begin{aligned}
u_{unit} &= u_F = \frac{1}{3}\frac{T\left(4L^3 + 6\pi L^2 R + 24LR^2 + 3\pi R^3\right)}{EI} \\
w_{unit} &= w_F = \frac{2TR(L^2 + 2R^2 + \pi LR)}{EI} \\
\alpha_{unit} &= \alpha_F = 0
\end{aligned} \tag{9}
$$

From the above equation, we can find the rotation angle of the beam cross section will be zero again after a whole unit, which means for the next unit the previous unit will not affect its global deflection by the rigid translation. It is caused by the symmetrical internal bending moment in the whole corrugation unit. Thus the global deflections of *n* units can be expressed as

$$
\begin{aligned}
u_n &= n \cdot u_{unit} \\
w_n &= n \cdot w_{unit}
\end{aligned} \tag{10}
$$

The deflections and beam cross section rotation angle of the different points in the trapezoidal and round corrugation unit are listed in the Table 1, 2, and 3. In the tables we can find the beam cross section rotation angles are symmetrical about the centre line of the corrugation unit.

Trapezoidal corrugation unit		Round corrugation unit	
Point	Axial deflections $u_i \ \ i = A, B, C, ...G$	Point	Axial deflections $u_i \ \ i = A, B, C, ...F$
B	$-\frac{1}{6}\frac{Tl_1^3\left(\sin\theta\right)^2}{EI}$	*B*	$-\frac{1}{6}\frac{TL^3}{EI}$
C	$-\frac{1}{6}\frac{Tl_1^3\left(\sin\theta\right)^2}{EI}$	*C*	$\frac{1}{6}\frac{T\left(-L^3 + 12LR^2 + 3\pi R^3\right)}{EI}$
D	$\frac{1}{3}\frac{Tl_1^2\left(\sin\theta\right)^2\left(2l_1 + 3l_2\right)}{EI}$	*D*	$\frac{1}{2}\frac{T\left(3L^3 + 4\pi L^2 R + 12LR^2 + \pi R^3\right)}{EI}$
E	$\frac{1}{2}\frac{Tl_1^2\left(\sin\theta\right)^2\left(3l_1 + 4l_2\right)}{EI}$	*E*	$\frac{1}{2}\frac{T\left(3L^3 + 4\pi L^2 R + 16LR^2 + 2\pi R^3\right)}{EI}$
F	$\frac{1}{2}\frac{Tl_1^2\left(\sin\theta\right)^2\left(3l_1 + 4l_2\right)}{EI}$	*F*	$\frac{1}{3}\frac{T\left(4L^3 + 6\pi L^2 R + 24LR^2 + 3\pi R^3\right)}{EI}$
G	$\frac{2}{3}\frac{Tl_1^2\left(\sin\theta\right)^2\left(2l_1 + 3l_2\right)}{EI}$		

Table 1. Axial deflections in the corrugation unit

Point	Rotation angle of the beam cross section	Vertical deflection $w_i \ = A, B, C, ...G$
B	$\frac{1}{2}\frac{Tl_1^2 \sin\theta}{EI}$	$\frac{1}{6}\frac{Tl_1^3 \sin\theta\cos\theta}{EI}$
C	$\frac{1}{2}\frac{Tl_1 \sin\theta\left(l_1 + 2l_2\right)}{EI}$	$\frac{1}{6}\frac{Tl_1 \sin\theta\left(l_1^2\cos\theta + 3l_1 l_2 + 3l_2^2\right)}{EI}$
D	$\frac{Tl_1 \sin\theta(l_1 + l_2)}{EI}$	$\frac{1}{2}\frac{Tl_1 \sin\theta\left(2l_1^2\cos\theta + 2l_1 l_2\cos\theta + l_1 l_2 + l_2^2\right)}{EI}$

E	$\frac{1}{2}\frac{Tl_1 \sin\theta\left(l_1+2l_2\right)}{EI}$	$\frac{1}{6}\frac{Tl_1 \sin\theta\left(11l_1^2\cos\theta+12l_1l_2\cos\theta+3l_1l_2+3l_2^2\right)}{EI}$
F	$\frac{1}{2}\frac{Tl_1^2 \sin\theta}{EI}$	$\frac{1}{6}\frac{Tl_1 \sin\theta\left(11l_1^2\cos\theta+12l_1l_2\cos\theta+6l_1l_2+6l_2^2\right)}{EI}$
G	0	$\frac{Tl_1 \sin\theta(l_1+l_2)(2l_1\cos\theta+l_2)}{EI}$

Table 2. Rotation of the beam cross section and vertical deflections in the trapezoidal corrugation unit

Point	Rotation angle of the beam cross section	Vertical deflection $w_i \;\; i = A, B, C, ...F$
B	$\frac{1}{2}\frac{TL^2}{EI}$	0
C	$\frac{1}{2}\frac{T\left(L^2+4R^2+2\pi LR\right)}{EI}$	$\frac{TR\left(L^2+2R^2+\pi LR\right)}{EI}$
D	$\frac{1}{2}\frac{T\left(L^2+4R^2+2\pi LR\right)}{EI}$	$\frac{TR\left(L^2+2R^2+\pi LR\right)}{EI}$
E	$\frac{1}{2}\frac{TL^2}{EI}$	$\frac{2TR\left(L^2+2R^2+\pi LR\right)}{EI}$
F	0	$\frac{2TR\left(L^2+2R^2+\pi LR\right)}{EI}$

Table 3. Rotation of the beam cross section and vertical deflections in the round corrugation unit

3. Verification of the Closed Form Modulii

The axial deflections are used to calculate the equivalent modulus in the axial direction. The equivalent modulus in the axial direction can be expressed for the trapezoidal corrugation as

$$E_x = \frac{T/S}{u_{unit}/(2c)} = \frac{3EI\left(2l_1\cos\theta+l_2\right)}{Sl_1^2\left(\sin\theta\right)^2\left(2l_1+3l_2\right)} \tag{11}$$

where S is area of the cross section of the corrugation.

For the round corrugation we have

$$E_x = \frac{12EIR}{S\left(4L^3+6\pi L^2R+24LR^2+3\pi R^3\right)} \tag{12}$$

The axial equivalent modulii are then compared to those from existing methods and the finite element method. The finite element models are built in Abaqus [12]. To ensure accuracy, a mesh convergence study is first performed, which gives a mesh size 0.001 m. Both the Euler beam element $B33$ and the Timoshenko beam element $B31$ are used for the verification, which are labelled as 'FEM (A)' and 'FEM (B)' in Figures 4 and 5 respectively. The equivalent methods from [4, 7, 9] are applied for the comparisons. The corrugated panel is assumed to be made of Aluminum sheet with a width 0.01 m. Figure 4 shows the equivalent axial modulus of the trapezoidal corrugation panel with different corrugation shapes. The proposed method has results identical to those from [7] since in the reference the equivalent modulus was also obtained by calculating the deflection under extension loads, although only half of the corrugation was considered. The homogenous method has some differences to the

proposed method. Compared to the finite element method, all the analytical methods have some errors. The error could be relatively large when the plate becomes thick compared to the size of the trapezoid. Also the Euler beam element has closer results to the proposed method since the method uses the classical beam theory and no transverse shear in the beam is considered.

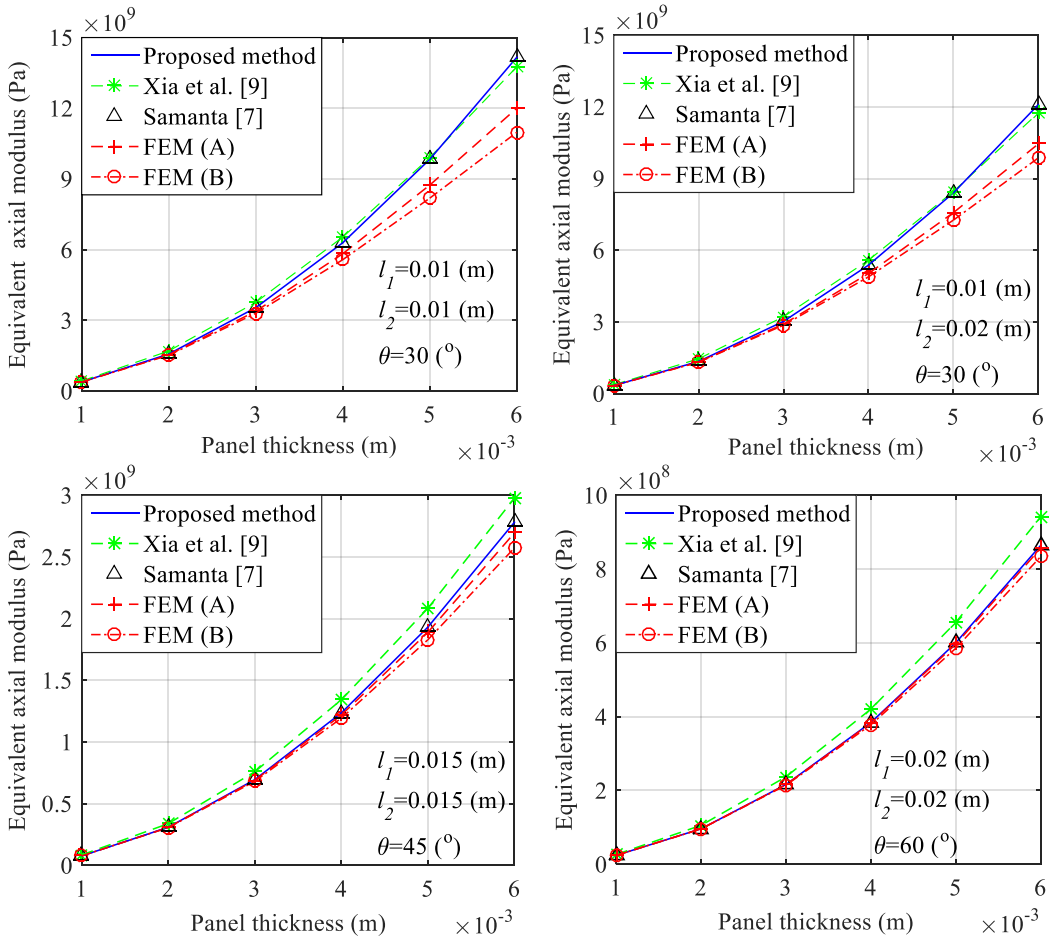

Figure 4. Equivalent axial modulus of the trapezoidal corrugation panel

The axial equivalent modulus of the round corrugation panel is shown in Figure 5. The homogenous method [9] provides very close results to the method proposed by Yokozeki et al. [4]. And the proposed method generally has a smaller error compared to the finite element than the trapezoidal corrugation panel, especially for the Euler beam element. The differences are due to the beam extension. The proposed method only considers the deflections caused by the bending of the beams. Figure 6 shows the results when the extension is considered. If the extension is included, the errors can be reduced significantly. Detailed analytical derivation also points out the extension has very small influence on the vertical deflections of trapezoidal corrugation panels and both axial and vertical deflections of round corrugation panels.

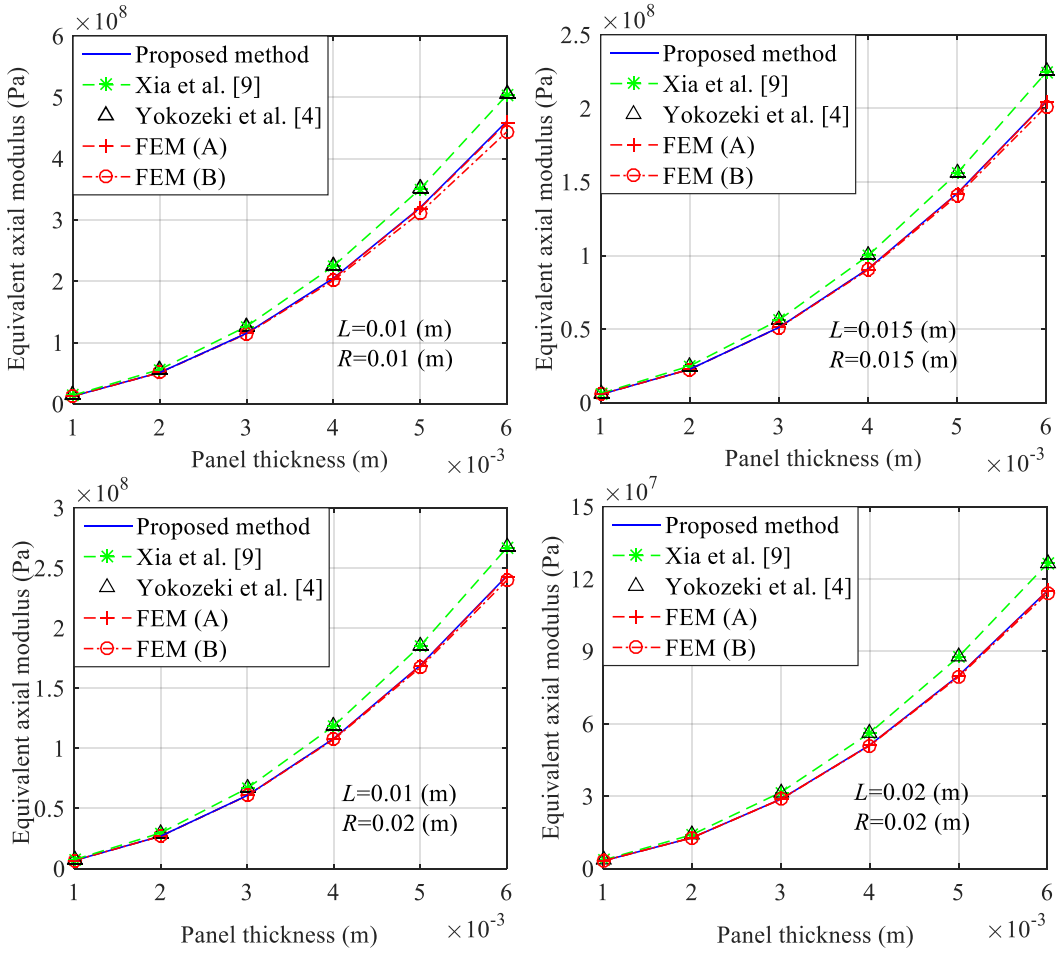

Figure 5. Equivalent axial modulus of the round corrugation panel

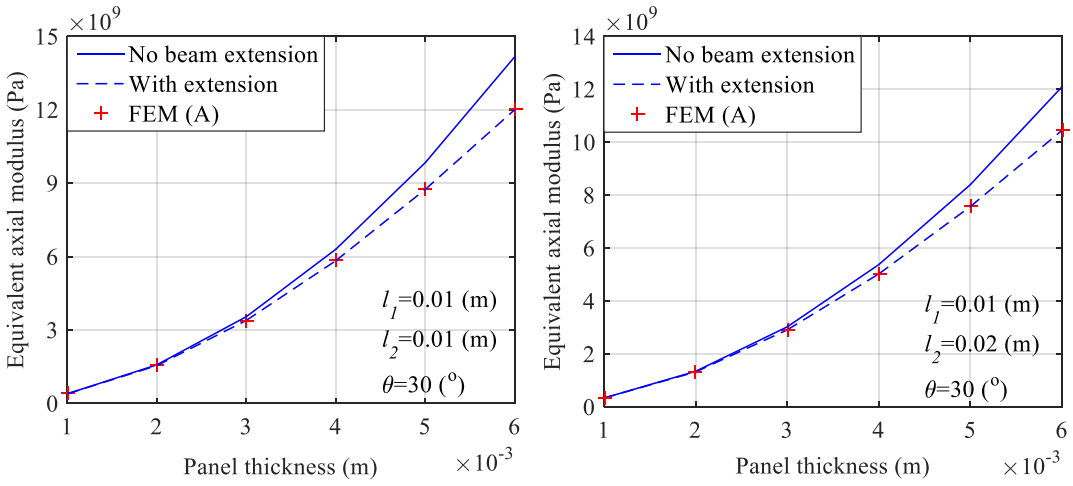

Figure 6. Influence of the beam extension on the equivalent axial modulus

Also we can represent the coupling stiffness K_c between the extension force and the vertical deflection of the corrugated panel as

$$K_c = \frac{T}{w_n} = \frac{T}{n \cdot w_{unit}} \tag{13}$$

For the trapezoidal corrugation

$$K_c = \frac{1}{n} \frac{EI}{l_1 \sin\theta \left(l_1 + l_2\right)\left(2l_1 \cos\theta + l_2\right)} \tag{14}$$

For the round corrugation

$$K_c = \frac{1}{n} \frac{EI}{2R\left(L^2 + 2R^2 + \pi LR\right)} \tag{15}$$

Then the vertical deflections of the corrugation panels are verified by the finite element method. Each finite element model has 10 units. The Euler beam element is used in the finite element model and the extension load is 1 N/mm. Figure 7 shows a linear relationship between the vertical deflection and the unit number. Different combinations of the shape of the corrugation unit are tested with the variable t representing the thickness of the corrugation panel. As shown in the figure the analytical solution has a good agreement with results obtained by the finite element model, which verifies the analytical expressions of the vertical deflection and coupling stiffness.

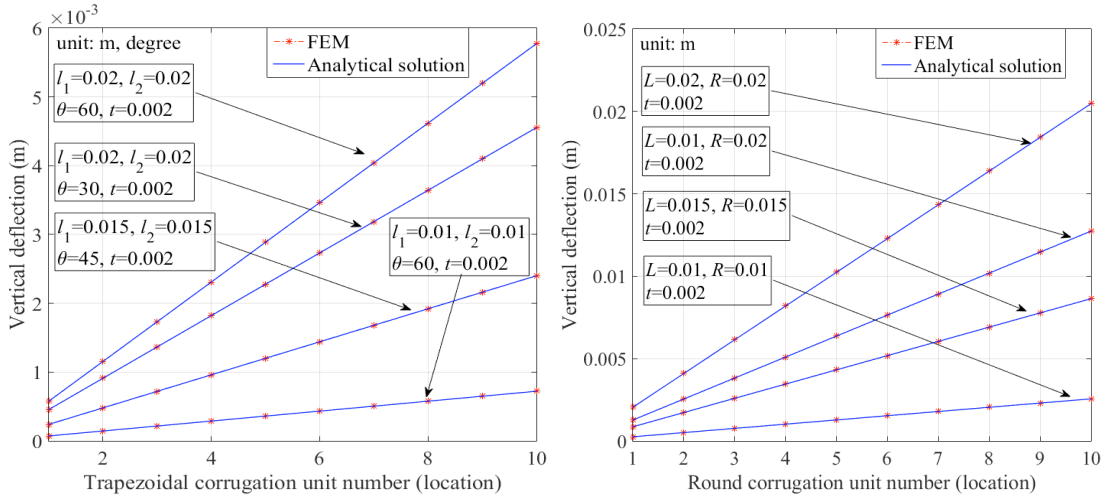

Figure 7. Vertical deflections verified by the FEM model, (a): Trapezoidal, (b): Round corrugation

A general equation can be used to express the axial and bending coupling effect. As shown in Figure 8, the corrugated panel is represented by two segments: the first corrugation unit which takes the boundary condition into account, and the second segment represents the rest of the corrugation units. Then the vertical deflection of the entire structure w_n can be expressed as

$$\begin{aligned} w_n &= \tan\gamma_{xz} \cdot L_n \\ \tan\gamma_{xz} &= \frac{w_1}{2c} \\ w_1 &= \begin{cases} 0 \left(\text{pinned boundary condition}\right) \\ w_{unit} \left(\text{fixed boundary condition}\right) \end{cases} \end{aligned} \tag{16}$$

where L_n is the length of the corrugated panel, and L_n=n·2c, and the vertical deflection of the first segment is denoted w_1.

By dividing the entire structure into two segments, the vertical deflection due to the fixed boundary condition can be represented by the rotation of the first segment. If the corrugated panel has a pinned boundary condition, no rotation angle will be generated. If the corrugated panel has a fixed boundary

condition, the rotation angle γ_{xz} of the first corrugated unit will be constant in the entire structure. This method makes the coupling an effect of the boundary condition, and the proposed modification a supplementary to the previous model.

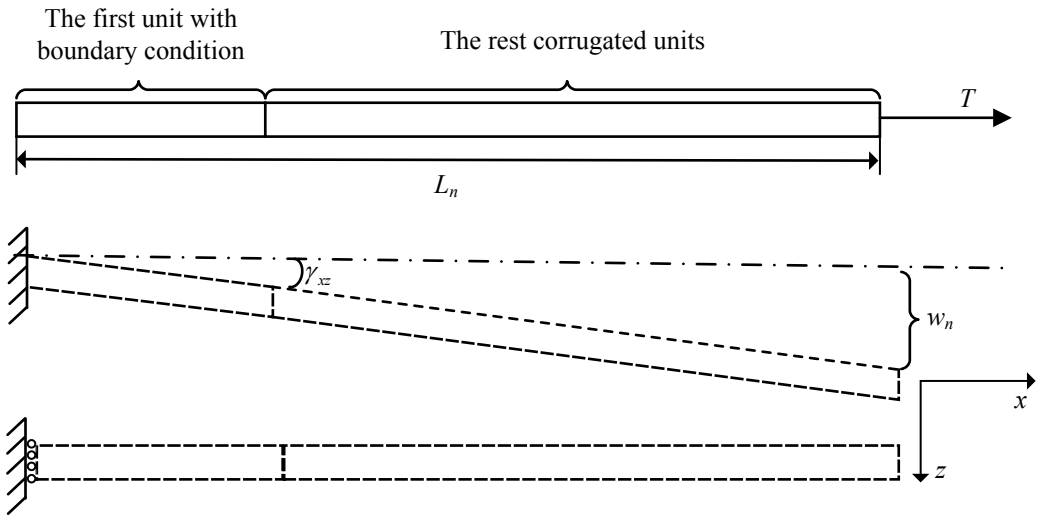

Figure 8. Vertical deflection under the pure extension load

A modification can be made to include the vertical deflection into the equivalent model. Another row (and column) is added to the global flexibility matrix on the basis of reference [9], in which $\overline{S}_{44}$ is the transverse component in the plane *xz* and $\overline{S}_{14}$ is the coupling component between the loading in the *x* direction and the shear strain in the *xz* plane.

$$\begin{Bmatrix} \overline{\varepsilon}_x \\ \overline{\varepsilon}_y \\ \overline{\gamma}_{xy} \\ \overline{\gamma}_{xz} \\ \overline{\kappa}_x \\ \overline{\kappa}_y \\ \overline{\kappa}_{xy} \end{Bmatrix} = \begin{bmatrix} \overline{S}_{11} & \overline{S}_{12} & 0 & \overline{S}_{14} & 0 & 0 & 0 \\ \overline{S}_{12} & \overline{S}_{22} & 0 & 0 & 0 & 0 & 0 \\ 0 & 0 & \overline{S}_{33} & 0 & 0 & 0 & 0 \\ \overline{S}_{14} & 0 & 0 & \overline{S}_{44} & 0 & 0 & 0 \\ 0 & 0 & 0 & 0 & \overline{S}_{55} & \overline{S}_{56} & 0 \\ 0 & 0 & 0 & 0 & \overline{S}_{56} & \overline{S}_{66} & 0 \\ 0 & 0 & 0 & 0 & 0 & 0 & \overline{S}_{77} \end{bmatrix} \begin{Bmatrix} \overline{N}_x \\ \overline{N}_y \\ \overline{N}_{xy} \\ \overline{N}_{xz} \\ \overline{M}_x \\ \overline{M}_y \\ \overline{M}_{xy} \end{Bmatrix} \tag{17}$$

When only extension load is applied, the load factor is $\begin{bmatrix} \overline{N}_x & 0 & 0 & 0 & 0 & 0 & 0 \end{bmatrix}^T$. The shear strain $\overline{\gamma}_{xz}$ is

$$\overline{\gamma}_{xz} = \overline{N}_x \overline{S}_{14} \tag{18}$$

Thus,

$$\overline{S}_{14} = \frac{\overline{\gamma}_{xz}}{\overline{N}_x} = \frac{a\tan\left(w_n / \left(n \cdot 2c\right)\right)}{\overline{N}_x} \tag{19}$$

where $\overline{N}_x$ is the force per unit width of the corrugated panel.

4. Method to eliminate the vertical deflection from extension

Section 3 investigates the vertical deflection caused by the extension loads when the corrugated panel has a fixed boundary condition. However this deflection is not wanted in some cases, such as span morphing or camber morphing applications, since the vertical deflection may change the aerodynamic shape or increase the required actuation force. If pinned boundary conditions can be used in these cases, the vertical deflections can be eliminated. But in some cases it is necessary to apply fixed boundary conditions for corrugated panels. The following section provides a solution to eliminate the deflection. The concept is to use the opposite rotation angle of the beam cross section, which is able to introduce an opposite vertical deflection. The opposite beam rotation is obtained by providing an offset to the initial boundary condition. As shown in Figure 9, the offset of the corrugated panel l_0 generates the vertical deflection w_0 and rotation angle α_0.

The rotation angle α_0 will lead to the vertical deflection w_r in the opposite direction to w_n. Then the total vertical deflection with the offset boundary condition can be represented as

$$\begin{aligned} w_{offset} &= w_0 + w_r + w_n \\ &= w_0 + \alpha_0 \cdot L_n + w_n \end{aligned} \tag{20}$$

For the trapezoidal corrugation,

$$\begin{aligned} w_0 &= -\frac{Tl_0^3 \sin\theta}{3EI}\cos\theta \\ \alpha_0 &= -\frac{Tl_0^2 \sin\theta}{2EI}\cdot nL \end{aligned} \tag{21}$$

Then,

$$w_{offset} = -\frac{Tl_0^3 \sin(\theta)}{3EI}\cos(\theta) - \frac{Tl_0^2 \sin\theta}{2EI}\left(n\cdot 2c\right) + n\left(\frac{Tl_1 \sin\theta (l_1+l_2)(l_2+2l_1\cos\theta)}{EI}\right) \tag{22}$$

Making the above equation zero will give a cubic equation of l_0. For the round corrugation, we have

$$\begin{aligned} w_0 &= 0 \\ \alpha_0 &= -\frac{Tl_0^2}{2EI} \end{aligned} \tag{23}$$

$$w_{offset} = -\frac{Tl_0^2}{2EI}\left(n\cdot 4R\right) + n\frac{2TR\left(L^2+2R^2+\pi LR\right)}{EI} \tag{24}$$

Making the above equation zero, we can obtain the offset as

$$l_0 = \sqrt{L^2+2R^2+\pi LR} \tag{25}$$

The offset boundary condition will also affect the axial deflection, which changes the equivalent axial modulus. For the round corrugation panel, the axial deflection of the offset part is

$$u_0 = \frac{Tl_0^3}{3EI} \tag{26}$$

Thus, the change of the equivalent axial modulus is

$$\frac{u_0}{u_n} = \frac{u_0}{n\cdot u_{unit}} \tag{27}$$

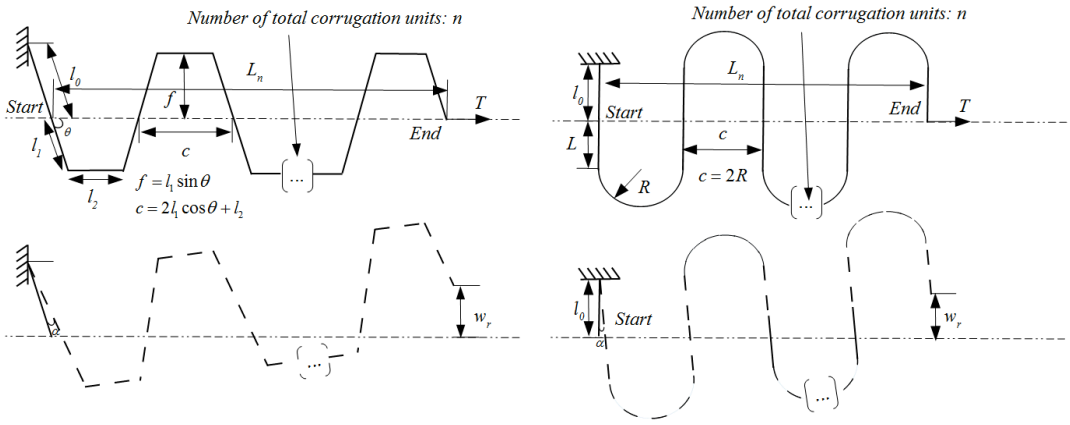

Figure 9. Offset boundary condition and the vertical deflection caused by the opposite rotation

5. Application to a morphing structure

A compliant structure has been proposed by the authors[13], in which the vertical deflection due to the extension force was not considered. As shown in Figure 10, the compliant structure consists of upper, lower and middle beams, which are represented as *AB*, *DC* and *BC*.

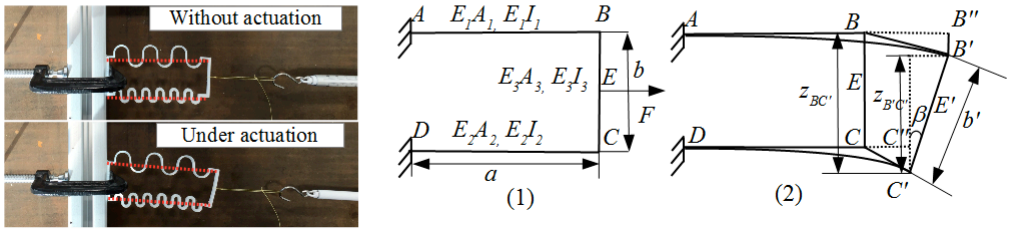

Figure 10. A compliant structure making use of the unsymmetrical stiffness of a corrugation panel

As shown by the red dashed lines in Figure 10, if the upper and lower beams have unsymmetrical stiffness ($E_1A_1<E_2A_2$), rotation of the structure can be induced by linear actuation. Analytical equations have been derived, and details of the derivation can be found in the appendix. But the coupling effect of the extension force and the vertical deflection is not included, which causes errors between the analytical results and the finite element method. According to the early study, the axial and vertical deflection u_E and v_E of the compliant structure can be expressed as

$$u_E = \frac{F}{2} a \frac{2E_1I_1 + 2E_2I_2 + \frac{b^2}{2}(E_1A_1 + E_2A_2)}{K_t}$$
$$v_E = \frac{Fba^2}{2} \frac{E_2A_2 - E_1A_1}{2K_t} \tag{28}$$

where the term K_t is the combination of the axial and bending stiffness of both upper and lower beams, which can be expressed as

$$K_t = E_1A_1E_1I_1 + E_2A_2E_2I_2 + E_1A_1E_2I_2 + E_1I_1E_2A_2 + E_1A_1E_2A_2b^2 \tag{29}$$

E_1, A_1, I_1, E_2, A_2, I_2, E_3, A_3, I_3 are the modulus, area and second moment of area of the upper, lower and middle beams respectively. The length and height of the structure are denoted a and b respectively. F is the actuation force. In the study the round corrugation panel is used as the upper and lower parts of the compliant structure. And the equivalent value of the corrugation panel should be applied to substitute the corresponding stiffness.

According to Equation (28), no vertical deflection should be obtained when the upper and lower beams have the same extension stiffness (E_1A_1=E_2A_2). However results from the detailed finite element models have shown differences. Modification is made to include the vertical deflection caused by the extension force.

The new prediction of the vertical deflection of compliant structure consists of two components, namely the original deflection calculated from Equation (28) and the vertical deflection due to the extension force. As shown in Figure 10, the vertical deflections of point B and C, i.e., $v_B^{'}$ and $v_C^{'}$, satisfy the relationship as

$$\begin{aligned} z_{B^{'}C^{'}} &= b^{'}\cos\beta \\ z_{B^{'}C^{'}} &= z_{BC^{'}} - B^{''}B^{'} = b + C^{''}C^{'} - B^{''}B^{'} = b + v_C^{'} - v_B^{'} \end{aligned} \tag{30}$$

Then we have

$$v_C^{'} - v_B^{'} = b^{'}\cos\beta - b \tag{31}$$

where $b^{'}$ is the deformed length of BC, β is the inclined angle of the middle beam BC. If the middle beam BC is assumed to be rigid enough, we can obtain

$$v_B^{'} = v_C^{'} \tag{32}$$

From the early study, we determined that the original vertical deflections of points B and C are the same, and thus the vertical deflections of points B and C due to its extension force v_{BM} and v_{CM} are also the same. Then, the upper and lower corrugated panel in the compliant structure can be regarded as two parallel springs under the extension force F. Thus we have

$$\begin{aligned} v_{BM} &= \frac{AX_1}{K_c^{upp}} \\ v_{CM} &= \frac{X_1}{K_c^{low}} \end{aligned} \tag{33}$$

where K_c is the coupling stiffness of the corrugated panel. The superscript '*upp*' and '*low*' correspond to the stiffness of the upper and lower beams. AX_1 and X_1 are the extension forces in the two corrugated panels. Since AX_1+X_1=F, we can deduce the equivalent stiffness of the compliant structure K_{eq}

$$K_{eq} = K_c^{upp} + K_c^{low} \tag{34}$$

Then the vertical deflection of the compliant structure due to the extension force F is

$$v_{EM} = \frac{F}{K_c^{eq}} = \frac{F}{K_c^{upp} + K_c^{low}} \tag{35}$$

The modified analytical method is then compared to the finite element method, as well as the original analytical method. The finite element analysis is performed in Abaqus[12] and a rigid body constraint is applied to the vertical beam to simulate its rigidity. Mesh convergence has also been verified before the analysis and the general purpose shell element *S4R* in Abaqus is used since the element is able to simulate both thin and thick plates. The modified analytical solution is labelled as 'Method A' and the original analytical solution is labelled as 'Method B' in Figure 11.

Figure 11 shows four different cases with different combinations of shapes and number of units. The corrugated panel is supposed to be made of Aluminum and t_1 and t_2 are the thicknesses of the

upper and lower corrugated panels. The compliant structure is actuated by the force F=100 N and t_1 is equal to 0.002 m. The width of the structure is fixed at 0.01 m. The x axis represents the change of the ratio of the lower and upper panel thickness, which indicates the change of the stiffness asymmetry. We can conclude the modified method is able to predict the vertical deflections more accurately than the old analytical method, especially when the upper and lower corrugation panel has the same stiffness. It is found that the vertical deflection due to extension force can be even larger than the maximum deduced deformation from stiffness asymmetry in some cases, when the height of the compliant structure is 0.2 m, which highlights the importance of taking the effect into account in this application.

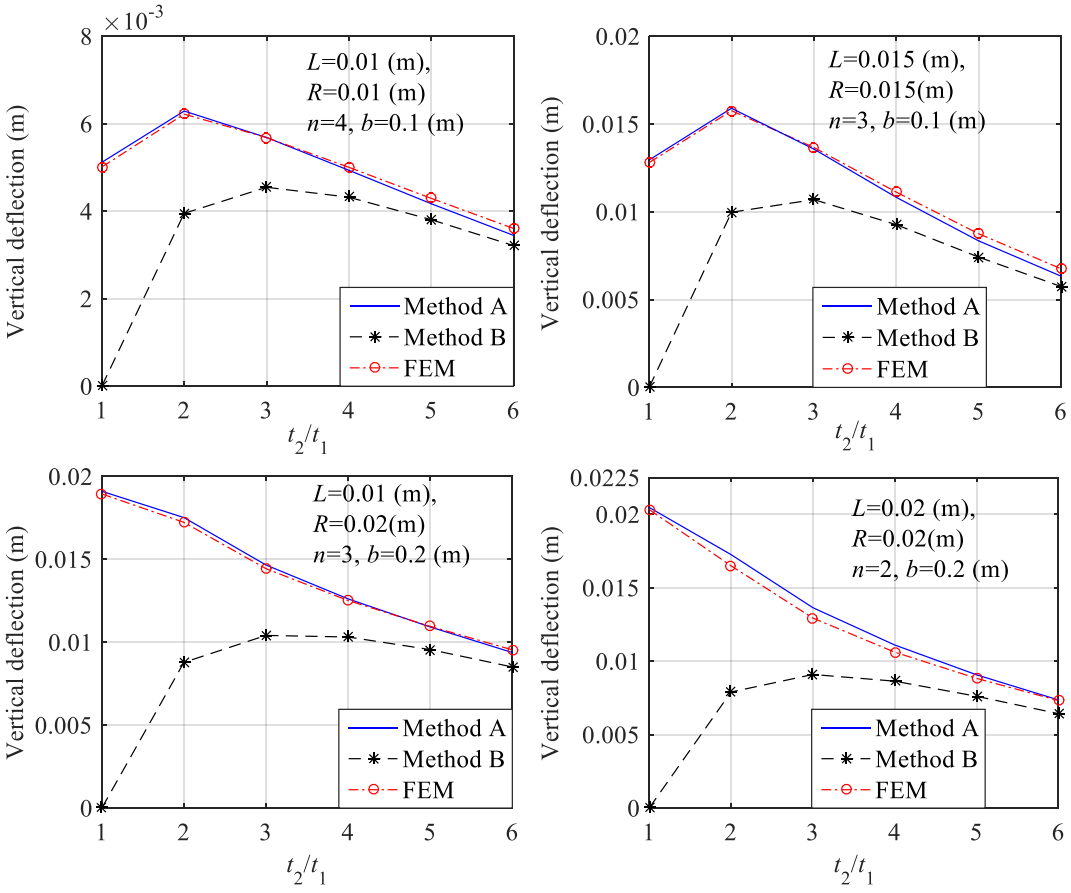

Figure 11. Vertical deflections of the compliant structure

6. Conclusion

In this paper, the vertical deflection under the pure extension load has been investigated when the corrugated panel has the fixed boundary condition, which is called axial and bending coupling of the corrugated panel. Trapezoidal and round corrugation panels are analysed. The corrugated panel is simplified as a two dimensional frame, which is made of classical beams. Detailed analysis of the internal bending moment shows the rotation angle of the beam cross sections and deflections of different points in the corrugated panel.

Analytical expressions of the vertical deflections are obtained by accumulating the local deflections and rigid translation due to beam rotation. The axial deflections are also obtained, which are applied to calculate the equivalent modulus in the axial direction. The deflections are verified by the existing methods in the literature and the finite element method. It is also found

that the beam extension needs to be considered for the prediction of the equivalent axial modulus of trapezoidal panels

The vertical deflection is found to be linear in terms of the number of corrugation units if the corrugated panel is assumed to be linear. In this case, the coupling between the vertical deflection and the pure extension load can be represented as an effect of the boundary condition of the corrugated panel. To include the coupling effect into the previous equivalent model, a coupling component is added to the equivalent flexibility matrix of the corrugated panel.

With the help of the modified model, the application of corrugated panels in morphing structures is shown. The importance of the coupling effect between the extension force and vertical deflection is highlighted in the study of a compliant structure. The differences between the analytical solution and the detailed finite element models can be reduced significantly if the coupling effect is taken into account. The approach to eliminate the vertical deflections is also introduced by providing an offset to the fixed boundary condition.

7. Reference

1. N. Buannic, P. Cartraud, and T. Quesnel, *Homogenization of corrugated core sandwich panels.* Composite Structures, 2003. **59**(3): p. 299-312.
2. A. Castrichini, V. Hodigere Siddaramaiah, D. Calderon, et al., *Nonlinear Folding Wing Tips for Gust Loads Alleviation.* Journal of Aircraft, 2016.
3. M. E. Biancolini, *Evaluation of equivalent stiffness properties of corrugated board.* Composite structures, 2005. **69**(3): p. 322-328.
4. T. Yokozeki, S.-I. Takeda, T. Ogasawara, et al., *Mechanical properties of corrugated composites for candidate materials of flexible wing structures.* Composites Part A: applied science and manufacturing, 2006. **37**(10): p. 1578-1586.
5. C. Thill, J. Etches, I. Bond, et al., *Composite corrugated structures for morphing wing skin applications.* Smart Materials and Structures, 2010. **19**(12): p. 124009-124018.
6. I. Dayyani, A. Shaw, E. S. Flores, et al., *The mechanics of composite corrugated structures: A review with applications in morphing aircraft.* Composite Structures, 2015. **133**: p. 358-380.
7. A. Samanta and M. Mukhopadhyay, *Finite element static and dynamic analyses of folded plates.* Engineering Structures, 1999. **21**(3): p. 277-287.
8. C. Thill, J. A. Etches, I. P. Bond, et al., *Investigation of trapezoidal corrugated aramid/epoxy laminates under large tensile displacements transverse to the corrugation direction.* Composites Part A: Applied Science and Manufacturing, 2010. **41**(1): p. 168-176.
9. Y. Xia, M. Friswell, and E. S. Flores, *Equivalent models of corrugated panels.* International Journal of Solids and Structures, 2012. **49**(13): p. 1453-1462.
10. H. Mohammadi, S. Ziaei-Rad, and I. Dayyani, *An equivalent model for trapezoidal corrugated cores based on homogenization method.* Composite Structures, 2015. **131**: p. 160-170.
11. I. Dayyani, M. I. Friswell, S. Ziaei-Rad, et al., *Equivalent models of composite corrugated cores with elastomeric coatings for morphing structures.* Composite Structures, 2013. **104**: p. 281-292.
12. *ABAQUS 6.13*, 2013, Dassault Systèmes
13. C. Wang, H. H. Khodaparast, and M. I. Friswell, *Investigating the benefits of morphing wing tip devices-A case study*

in *International Forum on Aeroelasticity and Structure Dynamics*2015: Saint Petersburg, Russia.

8. Appendix

This section shows the process of calculating the displacements of the proposed compliant structure. Since the upper and lower beams are fixed, there are six unknown reaction forces as shown in Figure A1, which are related to only three independent equations of equilibrium, thus the structure is statically indeterminate. The reaction forces applied at point D are chosen as redundant reactions. Then the structure becomes statically determinate with X_1, X_2, X_3 applied at point D.

To satisfy the original boundary condition, the redundant reactions will make the horizontal displacement u, vertical displacement v and rotation α at point D zero. Using the principle of superposition, u can be expressed as

$$u = u_F + u_{X_1} + u_{X_2} + u_{X_3} \tag{1}$$

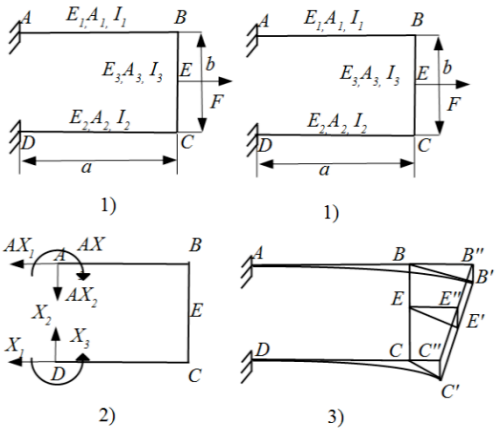

Figure A1. Redundant forces and the geometry relationship of point B, C, and E

where u_F is horizontal displacement caused by the actuation force F alone, and u_{X_i} $(i = 1,2,3)$ is the horizontal displacement caused by the reaction X_i alone.

According to the principle of virtual work, the displacement under an external load can be expressed as

$$u = \sum\int \frac{mM}{EI}dx + \sum\int \frac{nN}{EA}dx \tag{2}$$

where M and N are the bending moment and axial force under the external load, and m and n are the bending moment and axial force under the unit load applied in the same direction as the required displacement. Figure A2 shows the internal bending moment and axial force caused by F and the unit load, which is in the same direction to X_i (i=1, 2, 3). Thus, using the above equation, we obtain

$$\begin{aligned} u_F &= \sum\int \frac{mM}{EI}dx + \sum\int \frac{nN}{EA}dx \\ &= \int_0^a \frac{-b\cdot(\frac{1}{2}Fb)}{E_1 I_1}dx + \int_0^a \frac{-1\cdot F}{E_1 A_1}dx \\ &= -\frac{Fa}{E_1 A_1} - \frac{Fab^2}{2E_1 I_1} \end{aligned} \tag{3}$$

$$
\begin{aligned}
u_{X_1} &= \int_0^a \frac{1\cdot X_1}{E_1A_1}dx + \int_0^a \frac{1\cdot X_1}{E_2A_2}dx + \int_0^a \frac{b\cdot bX_1}{E_1I_1}dx \\
&= (\frac{a}{E_1A_1} + \frac{a}{E_2A_2} + \frac{ab^2}{E_1I_1})X_1
\end{aligned} \tag{4}
$$

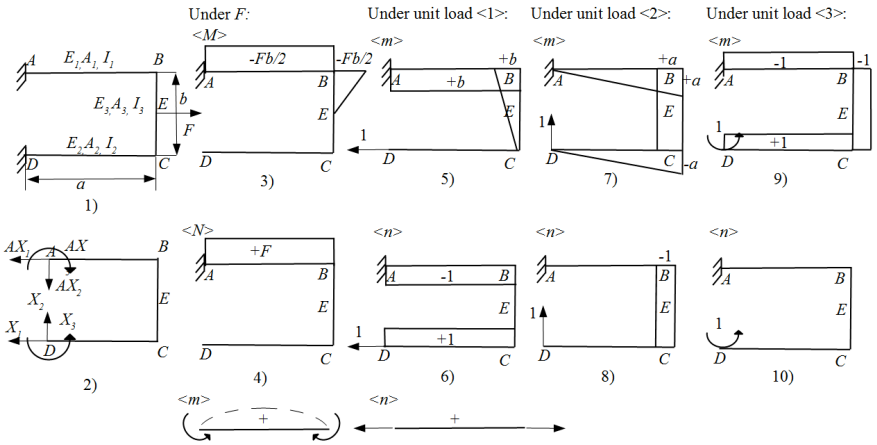

Figure A2. Reactions and internal loads

The same method can be used to get the other components of u, as well as the vertical displacement v and rotation α. Finally, at point D we obtain

$$
\begin{aligned}
u &= -\frac{Fa}{E_1A_1} - \frac{Fab^2}{2E_1I_1} + (\frac{ab^2}{E_1I_1} + \frac{a}{E_1A_1} + \frac{a}{E_2A_2})X_1 + \frac{a^2b}{2E_1I_1}X_2 - \frac{ab}{E_1I_1}X_3 \\
v &= -\frac{a^2b}{4E_1I_1}F + \frac{a^2b}{2E_1I_1}X_1 + (\frac{a^3}{3E_1I_1} + \frac{a^3}{3E_2I_2})X_2 - (\frac{a^2}{2E_1I_1} + \frac{a^2}{2E_2I_2})X_3 \\
\alpha &= \frac{Fab}{2E_1I_1} - \frac{ab}{E_1I_1}X_1 - (\frac{a^2}{2E_1I_1} + \frac{a^2}{2E_2I_2})X_2 + (\frac{a}{E_1I_1} + \frac{a}{E_2I_2})X_3
\end{aligned} \tag{5}
$$

Making the displacement and rotation at point D zero, the redundant reactions can be solved to give

$$
\begin{aligned}
X_1 &= \frac{E_2A_2(E_1A_1b^2 + 2E_1I_1 + 2E_2I_2)}{(E_1A_1E_1I_1 + E_2A_2E_2I_2 + E_1A_1E_2I_2 + E_1I_1E_2A_2 + E_1A_1E_2A_2b^2)}\frac{F}{2} \\
X_2 &= 0 \\
X_3 &= -\frac{E_2I_2(E_1A_1 - E_2A_2)}{(E_1A_1E_1I_1 + E_2A_2E_2I_2 + E_1A_1E_2I_2 + E_1I_1E_2A_2 + E_1A_1E_2A_2b^2)}\frac{Fb}{2}
\end{aligned} \tag{6}
$$

Then, we can obtain the reactions at point A from the equations of equilibrium as shown in Figure A3.

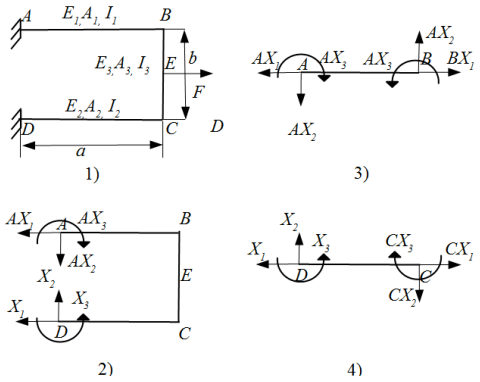

Figure A3. Balanced structure and beam AB and DC

According to the equilibrium of the whole structure,

$$\begin{aligned} F - AX_1 - X_1 &= 0 \\ AX_2 - X_2 &= 0 \\ AX_3 + X_1 b - \frac{1}{2} Fb - X_3 &= 0 \end{aligned} \tag{7}$$

Thus,

$$\begin{aligned} AX_1 &= \frac{E_1 A_1 (E_2 A_2 b^2 + 2E_1 I_1 + 2E_2 I_2)}{(E_1 A_1 E_1 I_1 + E_2 A_2 E_2 I_2 + E_1 A_1 E_2 I_2 + E_1 I_1 E_2 A_2 + E_1 A_1 E_2 A_2 b^2)} \frac{F}{2} \\ AX_2 &= 0 \\ AX_3 &= \frac{E_1 I_1 (E_1 A_1 - E_2 A_2)}{(E_1 A_1 E_1 I_1 + E_2 A_2 E_2 I_2 + E_1 A_1 E_2 I_2 + E_1 I_1 E_2 A_2 + E_1 A_1 E_2 A_2 b^2)} \frac{Fb}{2} \end{aligned} \tag{8}$$

Applying the equations of equilibrium to the upper and lower beams separately gives the internal forces and moments at point *B* and *C*, after which the displacements of point *B* and *C* can be obtained.

For the upper beam *AB*:

$$\begin{aligned} BX_1 - AX_1 &= 0 \\ AX_2 - BX_2 &= 0 \\ AX_3 - BX_3 - BX_2 a &= 0 \end{aligned} \tag{9}$$

$$\begin{aligned} u_B &= BX_1 a / (E_1 A_1) \\ v_B &= -BX_3 a^2 / (2E_1 I_1) - BX_2 a^3 / (3E_1 I_1) \end{aligned} \tag{10}$$

So,

$$\begin{aligned} u_B &= \frac{a\left[F - \dfrac{E_2 A_2 F (E_1 A_1 b^2 + 2E_1 I_1 + 2E_2 I_2)}{2K_t}\right]}{E_1 A_1} \\ &= \frac{F}{2} a \frac{2E_1 I_1 + 2E_2 I_2 + E_2 A_2 b^2}{K_t} \\ v_B &= \frac{a^2 \dfrac{Fb}{2}\left[\dfrac{E_2 A_2 (E_1 A_1 b^2 + 2E_1 I_1 + 2E_2 I_2)}{K_t} - 1 + \dfrac{E_2 I_2 (E_1 A_1 - E_2 A_2)}{K_t}\right]}{2E_1 I_1} \\ &= \frac{Fb}{2} a^2 \frac{E_2 A_2 - E_1 A_1}{2K_t} \\ K_t &= E_1 A_1 E_1 I_1 + E_2 A_2 E_2 I_2 + E_1 A_1 E_2 I_2 + E_1 I_1 E_2 A_2 + E_1 A_1 E_2 A_2 b^2 \end{aligned} \tag{11}$$

Here, the term K_t can be seen the combination of axial and bending stiffnesses of the upper and lower beams, and the term E_2A_2-E_1A_1 is the difference of the axial stiffnesses.

For the lower beam *DC*:

$$\begin{aligned} CX_1 - X_1 &= 0 \\ CX_2 - X_2 &= 0 \\ CX_3 + CX_2 a - X_3 &= 0 \end{aligned} \tag{12}$$

$$\begin{aligned} u_C &= \frac{CX_1 a}{E_2 A_2} \\ v_C &= \frac{CX_3 a^2}{2E_2 I_2} + \frac{CX_2 a^3}{3E_2 I_2} \end{aligned} \tag{13}$$

Thus

$$u_C = \frac{F}{2} a \frac{2E_1 I_1 + 2E_2 I_2 + E_1 A_1 b^2}{K_t}$$
$$v_C = \frac{Fb}{2} a^2 \frac{E_2 A_2 - E_1 A_1}{2K_t} \tag{14}$$

Point E is the midpoint of beam BC. As shown in Figure A1, $BB^{''}$, $CC^{''}$, $EE^{''}$ are the horizontal displacements of points B, C and E respectively, and $B^{''}B^{'}$, $E^{''}E'$, $C^{''}C'$ are the vertical displacements of points B, C and E. According to the geometry relationship,

$$\begin{aligned} u_E &= \frac{u_B + u_C}{2} \\ &= \frac{F}{2} a \frac{2E_1 I_1 + 2E_2 I_2 + \frac{b^2}{2}(E_1 A_1 + E_2 A_2)}{K_t} \\ v_E &= \frac{v_B + v_C}{2} \\ &= \frac{Fba^2}{2} \frac{E_2 A_2 - E_1 A_1}{2K_t} \end{aligned} \tag{15}$$